A Simple Deadbeat Predictive Current Control for OW-PMSM Drives Based on Reference Voltage Redistribution

Han Zhang and Xiaoguang Zhang, *Senior Member, IEEE*

***Abstract*—Zero-sequence current (ZSC), which inherently exists in the open-winding permanent magnet synchronous motor (OW-PMSM) with a common dc bus, would deteriorate the control performance of the system and add additional losses. Conventional proportional-integral (PI) controller involves the simultaneous adjustment of several parameters, which is an extremely time-consuming process. To solve these problems, this article proposes a simple deadbeat predictive current control (DPCC). First, a reference voltage weight factor is designed to redistribute the reference voltage of the dual-inverter, which makes the zero-sequence voltage generated by the nonzero voltage vector (VV) and the third harmonic back electromotive force cancel. Consequently, ZSC can be completely suppressed. Second, the zero VV u_7(111) are excluded from the modulation, so the switching frequency of the dual-inverter and common mode voltage can be effectively reduced. Meanwhile, the effective modulation range is analyzed in this article, which reveals the relationship between the ratio of the third harmonic flux linkage and the modulation index. Finally, the effectiveness and advantages of the proposed method are verified on a 1.25-kW OW-PMSM experimental platform.**

***Index Terms*—Deadbeat predictive current control (DPCC), open-winding permanent magnet synchronous motor (OW-PMSM), zero-sequence current (ZSC).**

I. Introduction

PERMANENT magnet synchronous motor (PMSM), as a typical ac motor, has gained significant importance in industry applications due to its small volume, high power density, and superior operating performance [1], [2], [3], [4]. However, classical PMSM fed by a single inverter is constrained in high-power and high-voltage applications, such as electric vehicles, rail traction, and aerospace. Under limited dc voltage source, an open-winding permanent magnet synchronous motor (OW-PMSM) is considered as an alternative solution for a high-power drive system [5], [6], [7], [8].

Manuscript received 13 November 2023; revised 22 January 2024; accepted 25 February 2024. Date of publication 29 February 2024; date of current version 19 April 2024. This work was supported in part by the National Natural Science Foundation of China under Grant 52377036 and in part by the Outstanding Talents Project of North China University of Technology. Recommended for publication by Associate Editor H. Chaoui. *(Corresponding author: Xiaoguang Zhang.)*

The authors are with the Inverter Technologies Engineering Research Center of Beijing, North China University of Technology, Beijing 100144, China (e-mail: zhangxg123456789@163.com; 1638762631@qq.com).

Color versions of one or more figures in this article are available at https://doi.org/10.1109/TPEL.2024.3371467.

Digital Object Identifier 10.1109/TPEL.2024.3371467

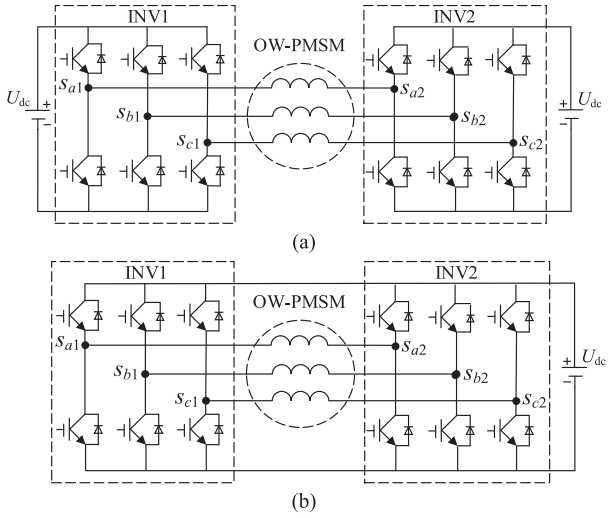

Fig. 1. Topology of OW-PMSM. (a) Isolated DC bus type. (b) Common DC bus type.

As a novel topology, OW-PMSM, which is powered by the dual-inverter has been extensively investigated in recent years.

Notably, the capacity of the conventional star-connected inverter is distributed to two inverters, which reduces the capacity of a single inverter and realizes multilevel modulation of the phase voltage compared to the classical PMSM. Generally, the drive topology of OW-PMSM can be classified into isolated dc bus type [9], [10] and common dc bus type [10], [11] according to whether the dual-inverter shares a common dc-voltage source, as shown in Fig. 1. It can be seen that two electrically isolated dc voltage sources are required in Fig. 1(a), which makes the system structure complex and increases the size and cost. In addition, another potential issue that may exist in the OW-PMSM system with the isolated dc bus is that the bus voltage on both sides are not equal, which may prevent the original control algorithm from working. The latter, which requires only a single dc voltage source, compensates for these problems extremely effectively. The simplified system with reduced cost makes it quickly become a major research hotspot for high-power drives.

However, the natural constraint that the vector sum of the three-phase currents is zero is broken owing to the direct connection of the two dc-links, which introduces a flow path for zero-sequence current (ZSC). As shown in Fig. 2, the zero-sequence voltage (ZSV), which is the difference between the common

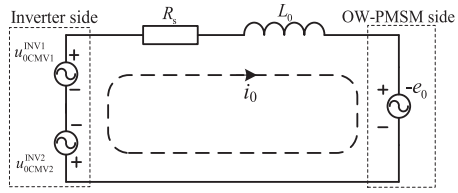

Fig. 2. Zero-sequence loop.

mode voltage (CMV) of the dual-inverter, and the third harmonic back electromotive force (EMF) at the motor side together form the zero-sequence loop [12]. ZSC is an unexpected component, which would increase the system losses and jeopardize the safe operation of the motor. As a result, additional ZSC suppression is required.

Over the years, the ZSC suppression strategies for OW-PMSM with a common dc bus are mainly divided into hardware and software solutions. The series saturated reactor is designed in [13] to suppress ZSC by increasing the zero-sequence impedance. In [14] and [15], the additional auxiliary switching tubes are designed in topology to achieve ZSC suppression. However, the reactors and switching tubes added to the system would increase the size and cost, which is limited in practical application. Therefore, the software approach to suppress ZSC is more competitive and easier to implement. The modified space vector pulsewidth modulation (SVPWM) with zero voltage vector (VV) redistribution is presented in [16], which makes the ZSV and the back EMF cancel each other. Literature [17] proposes a novel dual-space vector control method to suppress ZSC through zero VV redistribution in a single-side inverter. Consequently, ZSC can be effectively suppressed and the superior steady-state performance can be obtained in both methods. However, the high switching frequency, which leads to larger switching losses, is still a problem to be optimized. On this basis, the influence of ZSC on torque ripple is discussed in [18] and an additional current injection into the q-axis is introduced to compensate the torque ripple caused by ZSC. Furthermore, the switching frequency is reduced by phase-angle shift modulation, in which zero VV (111) is not required. Nevertheless, the phase current total harmonic distortion (THD) is severely worsened and the additional motor losses are increased. In [19], the duration time of three-phase pulses is readjusting in a control period, which suppresses ZSC and CMV simultaneously. Thus, a satisfactory control effect can be obtained and the switching frequency can be further reduced without zero VV $u_7(111)$.

The above-mentioned methods are all concerned with obtaining an accurate ZSV generated by the dual-inverter. However, additional proportional resonant or proportional integral resonant (PIR) controller are required in the current loop to generate the zero-sequence reference voltage. Considering the proportional-integral (PI) controllers of the speed loop, the cotuning of several parameters is a quite laborious problem in practical occasions. Besides, the slower dynamic response performance is an aspect that needs to be improved.

In recent years, model predictive control (MPC) has stood out from the crowd in the field of motor drives by virtue of its simple structure, fast dynamic response, and multivariable constraint capabilities. As one of the MPC, finite control set MPC (FCS-MPC) selects discrete VVs to act on the motor through a predefined cost function. Literature [20] presents a VV optimization selection method, which decouples the voltages from the $\alpha\beta$- to the abc-axes and the suppression of ZSC and the optimal selection of VVs can be guaranteed. In [21], the influence of dead-zone on the control system is analyzed, and then, the dead-time of the inverter is redistributed optimally to improve the steady-state performance of the system. In addition, in order to reduce the impact of parameter mismatch on the prediction model, a robust two-vector model predictive control strategy is proposed in [22] based on the hysteresis controller, which enhances the robustness of the zero-sequence parameter mismatch. It can be seen that although the above-mentioned methods comparatively improve the control performance, the great computational burden is a problem that FCS-MPC has to face [23], [24].

Compared to FCS-MPC, a better control performance and a fixed switching frequency can be obtained with deadbeat predictive current control (DPCC), which is a typical of continuous control set MPC (CCS-MPC). Only the reference voltages are required to substitute into the fixed module SVPWM, in which the computational burden can be considerably reduced. Incorporating the idea of the deadbeat control, a novel four-segment-mode CCS-MPC is proposed in [25] and [26], which obtains an excellent control steady-state performance. The suppression of ZSC is achieved by redistributing the modulation sequence, besides, VVs are optimally ordered to reduce the switching frequency. Therefore, a switching frequency fixed at half the control frequency is obtained. In order to solve the asymmetric operation of OW-PMSM with an isolated dc bus when the voltages of the two dc-link voltages are not equal, literature [27] presents a novel voltage modulation strategy, where the inverter at the low-voltage is kept in a low-potential clamping state instead of the dual-inverter being clamped alternately. Consequently, the total voltage synthesis region becomes larger and the voltage synthesis capability is better. In addition, in [28], an adaptive sliding mode control-based zero-sequence observer is designed to predict ZSV and ZSC, and then a novel DPCC scheme with alternate subhexagonal center pulsewidth modulation strategy is proposed to suppress ZSC and torque ripple simultaneously.

Literature [29] proposes an improved ZSC hysteresis control-based DPCC, in which two VVs in the mid-hexagonal and an VV in the outer-hexagonal for compensating the ZSV are used for SVPWM. Although a good control effect can be obtained with the above methods, the zero VV $u_7(111)$ needs to be engaged to pulsewidth modulation in [25] and [26], which produces a larger shaft voltage and CMV. In addition, the adoption of sliding mode observer involves the design and adjustment of several parameters, and the implementation of the hysteresis controller is relatively complicated. The simpler the control algorithm is employed in practical engineering, the lower the failure rate and the cost of protection can be obtained. Therefore, a simple DPCC is proposed in this article, which utilizes the voltage synthesis characteristics of the dual-inverter to redistribute the reference voltage and the ZSV output by the dual-inverter can always

counteract the third harmonic back EMF. Consequently, ZSC can be completely suppressed. Besides, the switching frequency of the dual-inverter can be reduced by excluding the zero VV $u_7(111)$ from the modulation, which further reduces the shaft voltage and CMV of the system. This article is organized as follows. Section II provides the mathematical model of OW-PMSM. The proposed simple DPCC method with reference voltage redistribution is presented in Section III. In addition, the effective modulation range is also analyzed in this section. Finally, the validity of the proposed method is verified in Section IV.

II. Mathematical Model of OW-PMSM

The common dc bus type OW-PMSM system fed by a dual-inverter is presented in Fig. 1(b), which does not change the electromagnetic design of the classical PMSM. Consequently, the voltage model of PMSM is still applicable to OW-PMSM. Besides, the characteristic zero-sequence loop needs to be considered. The voltage equation of OW-PMSM under the $dq0$ rotating coordinate frame can be expressed as

$$\begin{aligned}\begin{bmatrix} u_\mathrm{d} \\ u_\mathrm{q} \\ u_0 \end{bmatrix} &= \begin{bmatrix} L_\mathrm{d} & 0 & 0 \\ 0 & L_\mathrm{q} & 0 \\ 0 & 0 & L_0 \end{bmatrix} \frac{d}{dt} \begin{bmatrix} i_\mathrm{d} \\ i_\mathrm{q} \\ i_0 \end{bmatrix} \\ &+ \begin{bmatrix} R_\mathrm{s} & -\omega_\mathrm{e} L_\mathrm{q} & 0 \\ \omega_\mathrm{e} L_\mathrm{d} & R_\mathrm{s} & 0 \\ 0 & 0 & R_\mathrm{s} \end{bmatrix} \begin{bmatrix} i_\mathrm{d} \\ i_\mathrm{q} \\ i_0 \end{bmatrix} \\ &+ \begin{bmatrix} 0 \\ \omega_\mathrm{e} \psi_\mathrm{f} \\ -3\omega_\mathrm{e} \psi_{\mathrm{f}3} \sin 3\theta_\mathrm{e} \end{bmatrix} \end{aligned} \tag{1}$$

where u_d, u_q, and u_0 represent the stator voltage under the $dq0$-axes; i_d, i_q, and i_0 represent the stator current under the $dq0$-axes; ω_e represents the electrical angular speed; θ_e represents the electrical angle; L_d, L_q, and L_0 represent the inductance under the $dq0$-axes, and $L_\mathrm{d} = L_\mathrm{q}$ in the surface-mounted PMSM; ψ_f and $\psi_{\mathrm{f}3}$, respectively, denote the fundamental flux linkage and third harmonic flux linkage component; R_s is winding resistance. In addition, $e_0 = 3\omega_\mathrm{e}\psi_{\mathrm{f}3}\sin 3\theta_\mathrm{e}$ is expressed as the third harmonic back EMF.

The time delay, which inherently exists in the practical system, would deteriorate the control performance of the system. Generally, one-step prediction is employed to compensate for the time delay of the control system. The current prediction can be realized by discrete (1) with the forward Euler technique, which is expressed as

$$\begin{aligned}\begin{bmatrix} i_\mathrm{d}(k+1) \\ i_\mathrm{q}(k+1) \\ i_0(k+1) \end{bmatrix} &= \begin{bmatrix} 1 - \frac{RT_\mathrm{s}}{L_\mathrm{d}} & \omega_\mathrm{e}(k)T_\mathrm{s} & 0 \\ -\omega_\mathrm{e}(k)T_\mathrm{s} & 1 - \frac{RT_\mathrm{s}}{L_\mathrm{q}} & 0 \\ 0 & 0 & 1 - \frac{RT_\mathrm{s}}{L_0} \end{bmatrix} \begin{bmatrix} i_\mathrm{d}(k) \\ i_\mathrm{q}(k) \\ i_0(k) \end{bmatrix} \\ &+ \begin{bmatrix} \frac{T_\mathrm{s}}{L_\mathrm{d}} & 0 & 0 \\ 0 & \frac{T_\mathrm{s}}{L_\mathrm{q}} & 0 \\ 0 & 0 & \frac{T_\mathrm{s}}{L_0} \end{bmatrix} \begin{bmatrix} u_\mathrm{d}(k) \\ u_\mathrm{q}(k) \\ u_0(k) \end{bmatrix} + \begin{bmatrix} 0 \\ -\frac{\omega_\mathrm{e}(k)\psi_\mathrm{f}T_\mathrm{s}}{L_\mathrm{q}} \\ \frac{e_0(k)T_\mathrm{s}}{L_0} \end{bmatrix} \end{aligned} \tag{2}$$

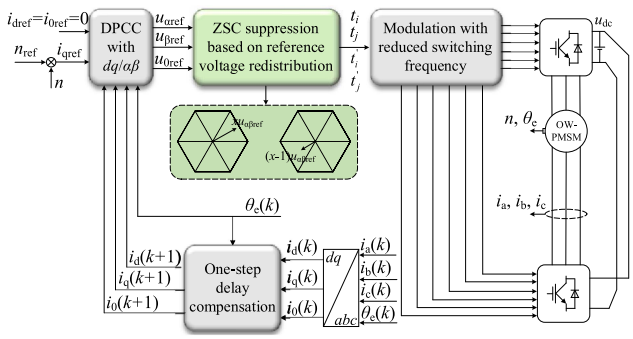

Fig. 3. Control diagram of the proposed simple DPCC.

where $i_{\mathrm{dq}0}(k+1)$ are denoted as the $dq0$-axes predicted current at the $(k+1)$th instant; $i_{\mathrm{dq}0}(k)$ are denoted as the sampled current.

Subject to ZSC, the electromagnetic torque of OW-PMSM can be expressed as

$$T_\mathrm{e} = \frac{3}{2} n_\mathrm{p} \left[\psi_\mathrm{f} i_\mathrm{q} + (L_\mathrm{d} - L_\mathrm{q}) i_\mathrm{d} i_\mathrm{q} - 6\psi_{\mathrm{f}3} i_0 \sin(3\theta_\mathrm{e})\right] \tag{3}$$

where n_p represents the pole pair of the motor. It can be seen in (3) that the ZSC is always presented as a sixth harmonic component in the torque. The smooth torque output is directly related to ZSC. Therefore, one of the most critical things, which needs to be addressed, is to suppress ZSC in the OW-PMSM system with a common dc bus.

III. Proposed Simple DPCC

From the above-mentioned analysis in Section I, ZSC is mainly composed of the ZSV generated by the pulsewidth modulation and the third back harmonic back EMF. The latter is expressed as a sinusoidal component varying with rotor position, which is uncontrolled. Fortunately, the ZSV output by the dual-inverter can be accurately modulated by using different VVs. As the only controlled voltage source, the VV with ZSVs of different polarities are commonly utilized in DPCC for pulsewidth modulation [22]. Besides, the reference voltage of the OW-PMSM is cosynthesized by dual-inverter, providing more flexible modulation characteristics. If the reference voltage of the system is available, the reference voltage of the two inverters can be skillfully assigned to obtain the desired ZSV. Unlike the average allocation of reference voltage in [26], this article presents a simpler method of reference voltage allocation that can consistently obtain the required ZSV to counteract the third harmonic EMF, as a result, ZSC can be completely suppressed. The overall diagram of the proposed DPCC is shown in Fig. 3, which mainly includes the calculation of the reference voltage, ZSC suppression based on the redistribution of the reference voltage and switching frequency optimization. The control strategy of $i_{\mathrm{dref}} = 0$ is used in this article and zero-sequence reference current $i_{0\mathrm{ref}}$ is set to 0.

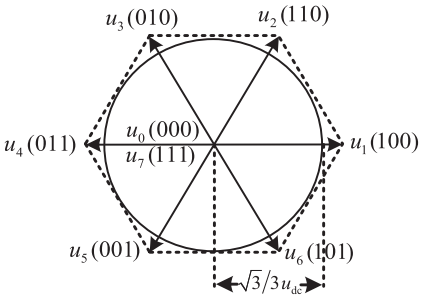

Fig. 4. Vector plane of single two-level inverter.

TABLE I
VOLTAGE VECTOR FOR A SINGLE INVERTER

VV		*Status*	u_α	u_β	u_0
	u_0	(000)	0	0	0
Odd VVs	u_1	(100)	$2U_{dc}/3$	0	$U_{dc}/3$
	u_3	(010)	$-U_{dc}/3$	$\sqrt{3}U_{dc}/3$	$U_{dc}/3$
	u_5	(001)	$-U_{dc}/3$	$-\sqrt{3}U_{dc}/3$	$U_{dc}/3$
Even VVs	u_2	(110)	$U_{dc}/3$	$\sqrt{3}U_{dc}/3$	$2U_{dc}/3$
	u_4	(011)	$-2U_{dc}/3$	0	$2U_{dc}/3$
	u_6	(101)	$U_{dc}/3$	$-\sqrt{3}U_{dc}/3$	$2U_{dc}/3$
	u_7	(111)	0	0	U_{dc}

For a single two-level inverter, the VV distribution plane is shown in Fig. 4, which consists of six nonzero VVs and two zero VVs. The voltage components under the $\alpha\beta$0-axes for each VV are shown in Table I, from which it can be seen that the odd VVs (u_1, u_3, u_5) can produce the ZSV of $U_{dc}/3$ and the even VVs can produce the ZSV of $2U_{dc}/3$.

A. ZSC Suppression With Reference Voltage Redistribution

As the most commonly used method of voltage distribution, the reference voltage is usually equally distributed to the dual-inverter for SVPWM. Despite its ease of implementation, ZSVs output by the dual-inverter are inherently limited. Consequently, an additional zero VV $u_7(111)$ injection is required to compensate for the ZSVs to suppress the ZSC [16]. However, it has been demonstrated in [30] and [31] that the high-frequency CMV of the system, which is expressed as half of the sum of the CMV for the dual-inverter, would generate unwanted shaft current and increase the system losses. In this article, the amplitude of the reference voltage of the dual-inverter is constantly jumped to maintain the dynamic balance between the ZSV generated by nonzero VVs and the third-harmonic back EMF. Consequently, the zero VV $u_7(111)$ can be avoided to participate in modulation to reduce the CMV.

According to the principle of deadbeat control ($i_{dq0}(k+2) = i_{dq0ref}$), the reference voltage of the system can be expressed as

$$\begin{bmatrix} u_{dref} \\ u_{qref} \\ u_{0ref} \end{bmatrix}$$

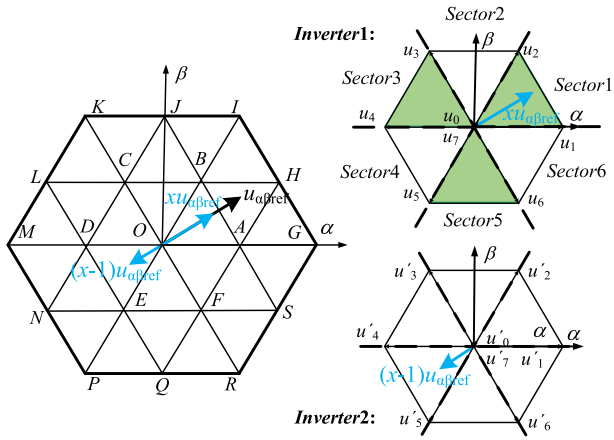

Fig. 5. Reference voltage redistribution.

$$= \begin{bmatrix} R_s - \frac{L_d}{T_s} & -\omega_e L_d & 0 \\ -\omega_e L_q & R_s - \frac{L_q}{T_s} & 0 \\ 0 & 0 & R_s - \frac{L_0}{T_s} \end{bmatrix} \begin{bmatrix} i_d(k+1) \\ i_q(k+1) \\ i_0(k+1) \end{bmatrix} + \begin{bmatrix} \frac{L_d}{T_s} & 0 & 0 \\ 0 & \frac{L_q}{T_s} & 0 \\ 0 & 0 & \frac{L_0}{T_s} \end{bmatrix} \begin{bmatrix} i_{dref} \\ i_{qref} \\ i_{0ref} \end{bmatrix} + \begin{bmatrix} 0 \\ \omega_e \psi_f \\ -3\omega_e \psi_{f3} \sin 3\theta_e \end{bmatrix}. \quad (4)$$

Through the inverse-Park transformation, the reference voltage under the $\alpha\beta$-axes can be obtained as

$$\begin{cases} u_{\alpha ref} = u_{dref}\cos(\theta_e) - u_{qref}\sin(\theta_e) \\ u_{\beta ref} = u_{dref}\sin(\theta_e) + u_{qref}\cos(\theta_e). \end{cases} \quad (5)$$

After obtaining the $\alpha\beta$-axes reference voltage, the reference voltage of the system needs to be assigned to the dual-inverter, and then two SVPWMs can be generated. In the OW-PMSM system, the total output voltage of the system is expressed as the voltage difference output by the two inverters

$$u_{\alpha\beta 0} = u_{\alpha\beta 0}^{INV1} - u_{\alpha\beta 0}^{INV2} \quad (6)$$

where $u_{\alpha\beta 0}^{INV1}$ and $u_{\alpha\beta 0}^{INV2}$ represent the ZSVs output by inverter1 (INV1) and inverter2 (INV2), respectively. Once the reference voltage of the dual-inverter has been obtained with the dichotomy of the reference voltage, the volt-second balance is used to ensure that the $\alpha\beta$-axes voltages are efficiently synthesized. However, the output ZSV is uniquely determined at the same time. Therefore, in order to ensure that the ZSV generated by the dual-inverter can be flexibly modulated, the reference voltage of the dual-inverter should be varied at all times according to (6). In this article, a weighting factor x is designed to redistribute the reference voltage of the dual-inverter, which satisfies $0<x<1$. The reference voltage of the dual-inverter can be expressed as

$$\begin{cases} u_{\alpha\beta ref}^{INV1} = x \cdot u_{\alpha\beta ref} \\ u_{\alpha\beta ref}^{INV2} = (x-1) \cdot u_{\alpha\beta ref} \end{cases}. \quad (7)$$

As shown in Fig. 5, the $x \cdot u_{\alpha\beta ref}$ is assigned to INV1 for SVPWM and $(1\text{-}x) \cdot u_{\alpha\beta ref}$ is assigned to INV2 for another SVPWM. According to the sector where the reference phase angle ($\theta_1 = \arctan(u_{\beta ref}^{INV1}/u_{\alpha ref}^{INV2})$) is located, two adjacent nonzero VVs can be selected for vector synthesis (one odd VV

and one even VV). The volt-second balance equation in INV1 can be expressed as

$$\begin{cases} xu_{\alpha\mathrm{ref}} \cdot T_\mathrm{s} = u_{\alpha-i}^{\mathrm{INV1}} \cdot t_i + u_{\alpha-j}^{\mathrm{INV1}} \cdot t_j \\ xu_{\beta\mathrm{ref}} \cdot T_\mathrm{s} = u_{\beta-i}^{\mathrm{INV1}} \cdot t_i + u_{\beta-j}^{\mathrm{INV1}} \cdot t_j. \end{cases} \tag{8}$$

In (8), $u_{\alpha\beta-i}^{\mathrm{INV1}}$ and $u_{\alpha\beta-j}^{\mathrm{INV1}}$ are denoted the $\alpha\beta$-axes voltage components of the two non-zero VVs, which can be obtained from Table I (i = 1, 3, 5; j = 2, 4, 6). t_i and t_j represent the durations of the two non-zero VVs, respectively, which can be further solved as

$$\begin{cases} t_i = x \cdot \dfrac{T_\mathrm{s}(u_{\beta-j}^{\mathrm{INV1}} \cdot u_{\alpha\mathrm{ref}} - u_{\alpha-j}^{\mathrm{INV1}} \cdot u_{\beta\mathrm{ref}})}{u_{\alpha-i}^{\mathrm{INV1}} \cdot u_{\beta-j}^{\mathrm{INV1}} - u_{\beta-i}^{\mathrm{INV1}} \cdot u_{\alpha-j}^{\mathrm{INV1}}} \\ t_j = x \cdot \dfrac{T_\mathrm{s}\left(u_{\beta-i}^{\mathrm{INV1}} \cdot u_{\alpha\mathrm{ref}} - u_{\alpha-i}^{\mathrm{INV1}} \cdot u_{\beta\mathrm{ref}}\right)}{u_{\alpha-j}^{\mathrm{INV1}} \cdot u_{\beta-i}^{\mathrm{INV1}} - u_{\beta-j}^{\mathrm{INV1}} \cdot u_{\alpha-i}^{\mathrm{INV1}}}. \end{cases} \tag{9a}$$

According to the sector symmetry, the duration of the two nonzero VVs in INV2 can be obtained as

$$\begin{cases} t_i^{'} = (x-1) \cdot \dfrac{T_\mathrm{s}(u_{\beta-j}^{\mathrm{INV2}} \cdot u_{\alpha\mathrm{ref}} - u_{\alpha-j}^{\mathrm{INV2}} \cdot u_{\beta\mathrm{ref}})}{u_{\alpha-i}^{\mathrm{INV2}} \cdot u_{\beta-j}^{\mathrm{INV2}} - u_{\beta-i}^{\mathrm{INV2}} \cdot u_{\alpha-j}^{\mathrm{INV2}}} \\ t_j^{'} = (x-1) \cdot \dfrac{T_\mathrm{s}\left(u_{\beta-i}^{\mathrm{INV2}} \cdot u_{\alpha\mathrm{ref}} - u_{\alpha-i}^{\mathrm{INV2}} \cdot u_{\beta\mathrm{ref}}\right)}{u_{\alpha-j}^{\mathrm{INV2}} \cdot u_{\beta-i}^{\mathrm{INV2}} - u_{\beta-j}^{\mathrm{INV2}} \cdot u_{\alpha-i}^{\mathrm{INV2}}}. \end{cases} \tag{9b}$$

In (9a) and (9b), only x is unknown, the durations t_i, t_j, $t_i^{'}$, and $t_j^{'}$would be affected by different weighting factor x. This further shows that the output ZSV of the dual-inverter can be flexibly changed by relying on tuning x, which is expressed as

$$u_{0\mathrm{output}} = \left[\frac{1}{3}U_\mathrm{dc}\left(t_i - t_i^{'}\right) + \frac{2}{3}U_\mathrm{dc}\left(t_j - t_j^{'}\right)\right] \cdot \frac{1}{T_\mathrm{s}}. \tag{10}$$

In order to suppress ZSC, a specific x must be obtained to make the ZSV output by the dual-inverter offset the third harmonic back EMF. Thus, the ZSV balance equation can be obtained as

$$u_{0\mathrm{output}} = \left[\frac{1}{3}U_\mathrm{dc}\left(t_i - t_i^{'}\right) + \frac{2}{3}U_\mathrm{dc}\left(t_j - t_j^{'}\right)\right] \cdot \frac{1}{T_\mathrm{s}} = u_{0\mathrm{ref}}. \tag{11}$$

In (11), the zero-sequence reference voltage $u_{0\mathrm{ref}}$ has been obtained by deadbeat algorithm in (4); t_i, t_j, $t_i^{'}$, and $t_j^{'}$ can be expressed by the weight factor x. Therefore, (11) can be transformed into solving a simple equation with respect to the weight factor x, which is calculated as follows:

$$x = \frac{(3u_{0\mathrm{ref}}/U_\mathrm{dc} - \mathrm{C} - 2\mathrm{D})}{(\mathrm{A} + 2\mathrm{B} - \mathrm{C} - 2\mathrm{D})} \tag{12}$$

where

$$\begin{cases} \mathrm{A} = \left(u_{\beta-j}^{\mathrm{INV1}} \cdot u_{\alpha\mathrm{ref}} - u_{\alpha-j}^{\mathrm{INV1}} \cdot u_{\beta\mathrm{ref}}\right) / \\ \qquad \left(u_{\alpha-i}^{\mathrm{INV1}} \cdot u_{\beta-j}^{\mathrm{INV1}} - u_{\beta-i}^{\mathrm{INV1}} \cdot u_{\alpha-j}^{\mathrm{INV1}}\right) \\ \mathrm{B} = \left(u_{\beta-i}^{\mathrm{INV1}} \cdot u_{\alpha\mathrm{ref}} - u_{\alpha-i}^{\mathrm{INV1}} \cdot u_{\beta\mathrm{ref}}\right) / \\ \qquad \left(u_{\alpha-j}^{\mathrm{INV1}} \cdot u_{\beta-i}^{\mathrm{INV1}} - u_{\alpha-i}^{\mathrm{INV1}} \cdot u_{\beta-j}^{\mathrm{INV1}}\right) \\ \mathrm{C} = \left(u_{\beta-j}^{\mathrm{INV2}} \cdot u_{\alpha\mathrm{ref}} - u_{\alpha-j}^{\mathrm{INV2}} \cdot u_{\beta\mathrm{ref}}\right) / \\ \qquad \left(u_{\alpha-i}^{\mathrm{INV2}} \cdot u_{\beta-j}^{\mathrm{INV2}} - u_{\beta-i}^{\mathrm{INV2}} \cdot u_{\alpha-j}^{\mathrm{INV2}}\right) \\ \mathrm{D} = \left(u_{\beta-i}^{\mathrm{INV2}} \cdot u_{\alpha\mathrm{ref}} - u_{\alpha-i}^{\mathrm{INV2}} \cdot u_{\beta\mathrm{ref}}\right) / \\ \qquad \left(u_{\alpha-j}^{\mathrm{INV2}} \cdot u_{\beta-i}^{\mathrm{INV2}} - u_{\beta-j}^{\mathrm{INV2}} \cdot u_{\alpha-i}^{\mathrm{INV2}}\right). \end{cases}$$

After obtaining the weight factor x, the x needs to be substituted into (9), and the duration of the two nonzero VVs can be obtained. Next, the remaining time is allocated to the zero VV u_0(000). Then two SVPWMs can be obtained.

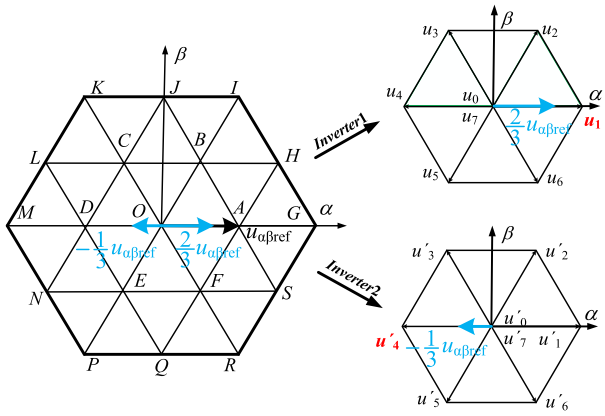

Fig. 6. Example with a reference voltage of $2/3U_\mathrm{dc}$ and located on the α^+-axis.

Define modulation index m as

$$m = \frac{|u_{\alpha\beta\mathrm{ref}}|}{2\sqrt{3}U_\mathrm{dc}/3}. \tag{13}$$

From the above-mentioned analysis, it can be seen that for a specific m under the modulation range, a particular weighting factor x can always be obtained to assign the reference voltage of the dual-inverter. As a result, the ZSVs generated by nonzero VV and the third harmonic back EMF are always in dynamic balance.

For example, assuming that the amplitude of the reference voltage is $2/3U_\mathrm{dc}$ and lies on the α^+-axis, the zero-sequence reference voltage is 0, as shown in Fig. 6. According to the volt-second balance principle, the following equation is given:

$$\frac{1}{3}U_\mathrm{dc} \cdot \frac{u_{\alpha\beta\mathrm{ref}}^{\mathrm{INV1}}}{2/3U_\mathrm{dc}} - \frac{2}{3}U_\mathrm{dc} \cdot \frac{u_{\alpha\beta\mathrm{ref}}^{\mathrm{INV2}}}{2/3U_\mathrm{dc}} = u_{0\mathrm{ref}} = 0. \tag{14}$$

Then, $u_{\alpha\beta\mathrm{ref}}^{\mathrm{INV1}} = 2u_{\alpha\beta\mathrm{ref}}^{\mathrm{INV2}}$ can be obtained according to (14). Therefore, to ensure that the ZSV output by the dual-inverter is 0, $2/3u_{\alpha\beta\mathrm{ref}}$ needs to be assigned to INV1 and $-1/3u_{\alpha\beta\mathrm{ref}}$ needs to be assigned to INV2, i.e., the weight factor x is set to 2/3.

The flowchart of the proposed ZSC suppression strategy is shown in Fig. 7. It can be seen in Fig. 7 that only a specific x needs to be computed to redistribute the reference voltage according to (11). Then, ZSC can be suppressed, which is simple and easy to implement.

B. Modulation With Switching Frequency Optimization

In Section III-A, a novel reference voltage redistribution strategy is presented to suppress ZSC, which makes the ZSV generated by the nonzero VV counteract the third harmonic back EMF. As a result, the zero VV u_7(111) that generates the ZSV of U_dc can be abandoned to involve in the pulsewidth modulation. The switching frequency of the dual-inverter can be effectively reduced by using only zero VV u_0(000).

Usually, one turn-ON and one turn-OFF of the switching tube are considered as an action. The average switching frequency is

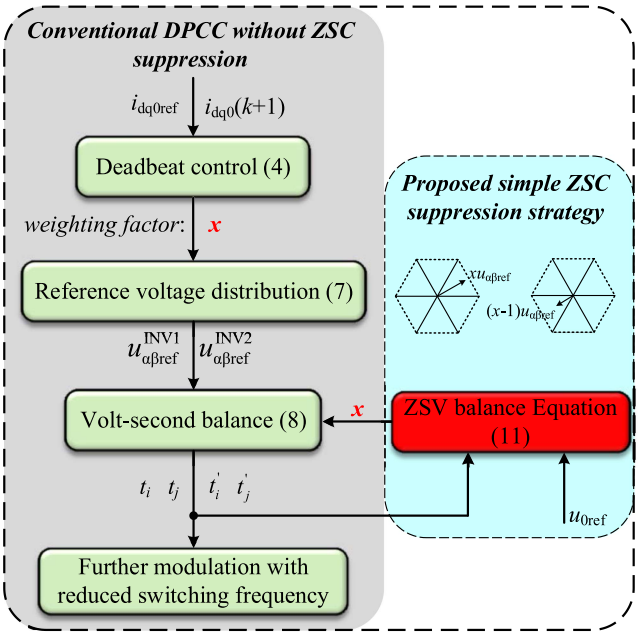

Fig. 7. Flowchart of the simplified SVPWM with ZSC suppression.

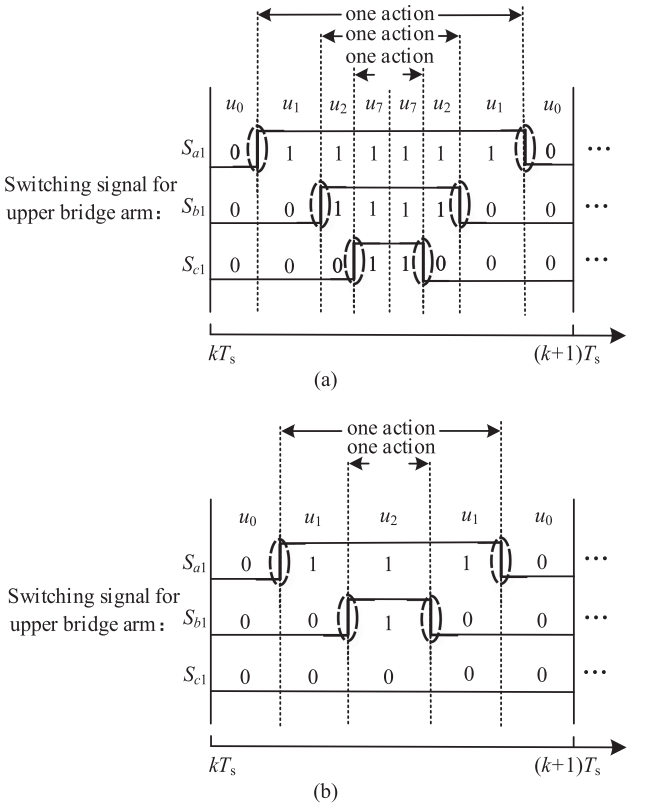

Fig. 8. Switching sequence. (a) Conventional SVPWM. (b) SVPWM with switching frequency optimization.

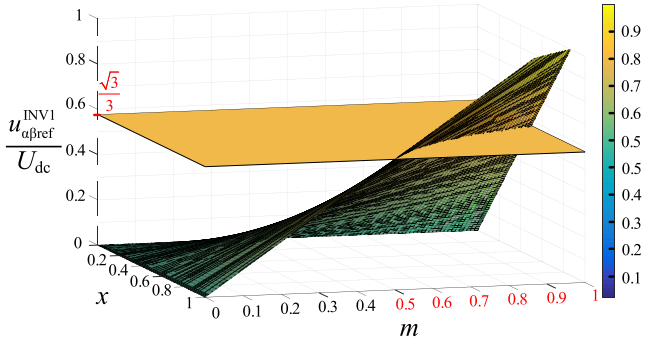

Fig. 9. Relationship between modulation index m and weighting factor x.

defined as the action times of six switching tubes per unit time. Take Fig. 8 as an example, when the conventional SVPWM is implemented, there are three actions for switching tubes in a single inverter, whereas there are only two actions in the proposed method. With the switching frequency optimization, the switching state of a particular phase bridge arm can always be clamped at 0. The average switching frequency of the dual-inverter is effectively reduced by 33%.

In addition, the high-frequency ZSV can cause shaft voltage, which would lead to premature bearing failure and affect the service life of the motor. The zero VV $u_7(111)$ is discarded to help reduce shaft voltage in the OW-PMSM system, especially for high-power applications.

C. Analysis of Modulation Range

In the proposed method, the point is to find a specific weighting factor x to balance the ZSV and the third harmonic back EMF with a given reference voltage. Combining (7) and (13), the relationship between x and m can be obtained as

$$\frac{u_{\alpha\beta\mathrm{ref}}^{\mathrm{INV1}}}{U_{\mathrm{dc}}} = \frac{2}{\sqrt{3}} m \cdot x. \tag{15}$$

For a single two-level inverter, the maximum synthesized voltage capacity of SVPWM is $\sqrt{3}/3U_{\mathrm{dc}}$. When the modulation index m satisfies $0<m<0.5$ (i.e., the amplitude of the total reference voltage $u_{\alpha\beta\mathrm{ref}}$ is less than $\sqrt{3}/3U_{\mathrm{dc}}$), the reference voltage of a single inverter can always be accurately modulated no matter how the reference voltage $u_{\alpha\beta\mathrm{ref}}$ is assigned. However, in the case of $0.5\leq m<1$ (i.e., the amplitude of the reference voltage $u_{\alpha\beta\mathrm{ref}}$ is greater than $\sqrt{3}/3U_{\mathrm{dc}}$), $xu_{\alpha\beta\mathrm{ref}}$ may exceed the voltage capacity of INV1 when the weighting factor x is sufficiently large, as shown in Fig. 9. The assigned reference voltage is no longer able to be accurately synthesized by a single inverter. In this case, the ZSC of the system cannot be effectively suppressed. Therefore, the analysis of the modulation range of ZSC is necessary.

According to the volt-second balancing principle, (9) can be transformed into an expression with respect to θ_e, x, and m. And then ZSV output by the dual-inverter, when $u_{\alpha\beta\mathrm{ref}}^{\mathrm{INV1}}$ is located in sector1 ($0\leq\theta_e\leq\pi/3$), can be obtained as

$$u_{0\mathrm{output}} = \left[xm\sin\theta_e + \left(\sqrt{3}xm - \frac{2\sqrt{3}}{3}m \right) \cos\theta_e \right] U_{\mathrm{dc}}. \tag{16}$$

It can be seen from (16) that different ZSV can be obtained by adjusting different x. For $m<0.5$, the maximum value of ZSV can

be obtained when the reference voltage $u_{\alpha\beta\mathrm{ref}}$ is fully assigned to INV1 with $x = u_{\alpha\beta\mathrm{ref}}^{\mathrm{INV1}}/u_{\alpha\beta\mathrm{ref}} = 1$. For $m \geq 0.5$, the maximum value of ZSV can be obtained when the reference voltage of INV1 is in critical modulation (i.e., $|u_{\alpha\beta\mathrm{ref}}^{\mathrm{INV1}}| = \sqrt{3}/3\, U_{\mathrm{dc}}$), in this case, $x = 1/(2m)$. Similarly, the minimum value of ZSV can be obtained according to the symmetry relation of the dual-inverter. Therefore, (16) can be rewritten as

$$\frac{[u_{0\mathrm{output}}]_{\max}}{U_{\mathrm{dc}}} = \begin{cases} \frac{1}{3}m\left(\sqrt{3}\cos\theta_{\mathrm{e}} + 3\sin\theta_{\mathrm{e}}\right) & m < 0.5 \\ \sin\left(\frac{\pi}{3} + \theta_{\mathrm{e}}\right) - \frac{2\sqrt{3}}{3}m\cos\theta_{\mathrm{e}} & m \geq 0.5. \end{cases} \tag{17a}$$

$$\frac{[u_{0\mathrm{output}}]_{\min}}{U_{\mathrm{dc}}} = \begin{cases} -\frac{2\sqrt{3}}{3}m\cos\theta_{\mathrm{e}} & m < 0.5 \\ \sin\left(\frac{\pi}{3} + \theta_{\mathrm{e}}\right) - \frac{1}{3}m\left(\sqrt{3}\cos\theta_{\mathrm{e}} + 3\sin\theta_{\mathrm{e}}\right) & m \geq 0.5. \end{cases} \tag{17b}$$

The above-mentioned analysis can be extended to the other five sectors, then the relationship between $u_{0\mathrm{output}}/U_{\mathrm{dc}}$ and θ_{e} can be obtained with different m, which is presented in Fig. 10. In Fig. 10, the range between the upper boundary of $u_{0\mathrm{output}}$ and the lower boundary of $u_{0\mathrm{output}}$ is called as the absolute modulation region. It can be seen that the absolute modulation region increases as m increases when $m < 0.5$ and decreases as m decreases when $m \geq 0.5$. The maximum ZSV can be obtained when $m = 0.5$, while the ZSV is compressed when the available reference voltage of INV2 starts to increase as m continues to increase. Moreover, it can also be noticed in Fig. 10 that, during the absolute modulation region, the minimum value of the upper boundary of the ZSV $[u_{0\mathrm{outputmax}}]_{\min}$ can always be obtained at $\theta_{\mathrm{e}} = 0,\ 2\pi/3,\ 4\pi/3$, the maximum value of the lower boundary of the ZSV $[u_{0\mathrm{outputmin}}]_{\max}$ can always be obtained at $\theta_{\mathrm{e}} = \pi/3,\ \pi,\ 5\pi/3$. The relationship between $[u_{0\mathrm{outputmax}}]_{\min}$, $[u_{0\mathrm{outputmin}}]_{\max}$ and the modulation index m is shown in Fig. 11, from which it can be seen that when m equals 0.75, the modulable ZSV boundary is zero. At this point, ZSC of the system cannot be effectively suppressed.

In addition, analyzing from the inverter-side, the modulated ZSV needs to counteract the third harmonic back EMF to completely suppress ZSC. The amplitude of the third harmonic back EMF is expressed as

$$E_0 = 3\omega_{\mathrm{e}}\psi_{\mathrm{f}}. \tag{18}$$

In (1), neglecting the u_{d}, voltage drop across the resistance and dynamic term in u_{q}, the following assumptions can be established:

$$u_{\alpha\beta\mathrm{ref}} = \sqrt{{u_{\mathrm{d}}}^2 + {u_{\mathrm{q}}}^2} = \omega_{\mathrm{e}}\psi_{\mathrm{f}}. \tag{19}$$

Combined (13) and (19), (18) can be rewritten as

$$E_0 = 3 \times \frac{2U_{\mathrm{dc}}}{\sqrt{3}} \times m \times \frac{\psi_{\mathrm{f3}}}{\psi_{\mathrm{f}}}. \tag{20}$$

Define the ratio of the third harmonic flux linkage to the fundamental component as k, it can be seen from (20) that the amplitude of the third harmonic back EMF is proportional to m and k. Different amplitudes of the third harmonic back EMF can be obtained with different k even in the case of the same m. Therefore, when k is set to 0.05, 0.1, 0.166, the relationship between the back EMF and modulation index m is presented in Fig. 12, from which it can be seen that the back EMF becomes larger as k increases. Thus, a maximum tolerable ratio of the third harmonic flux linkage can be obtained that makes the modulated

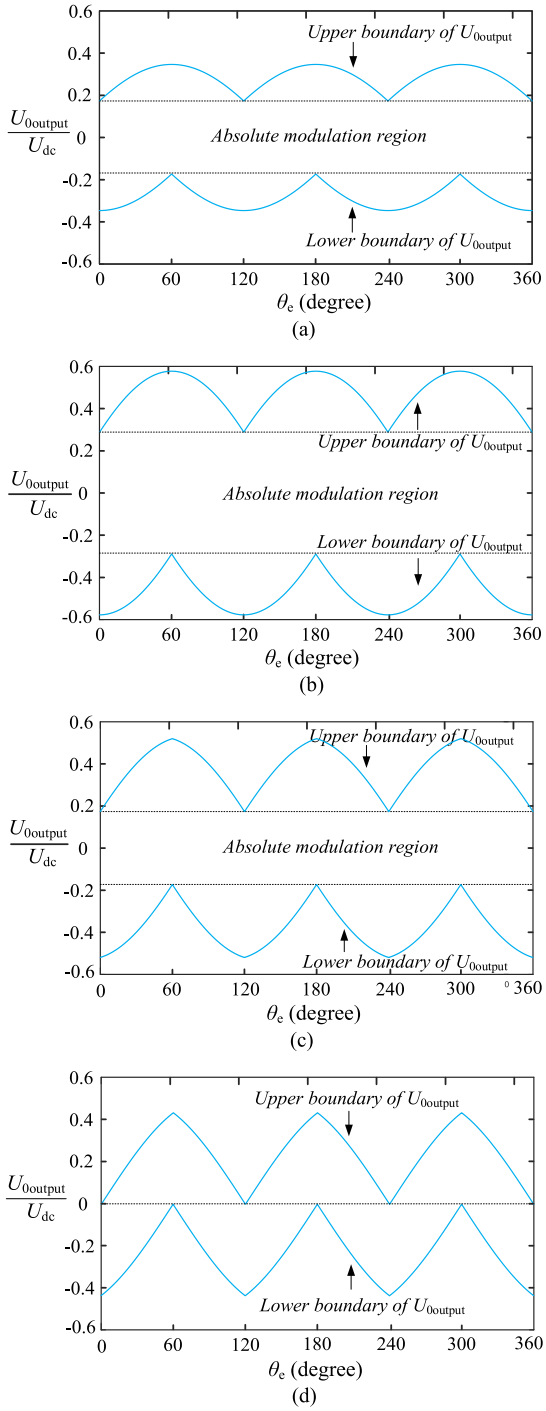

Fig. 10. ZSV modulation boundary. (a) $m = 0.3$. (b) $m = 0.5$. (c) $m = 0.6$. (d) $m = 0.75$.

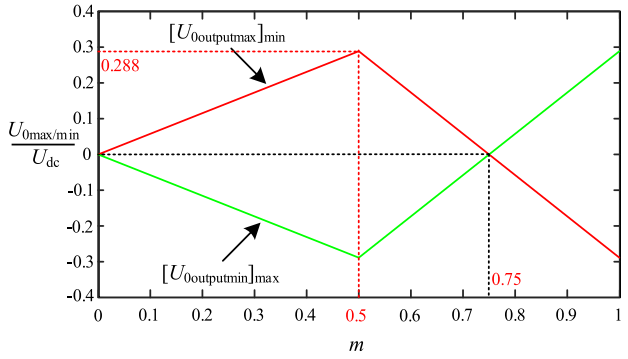

Fig. 11. Absolute modulation region with different m.

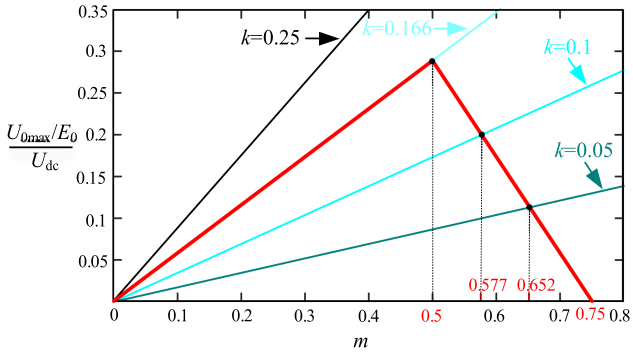

Fig. 12. Relationship between the maximum modulable ZSV and the third harmonic back EMF at different k.

ZSV and the back EMF counteract each other. In Fig. 12, the line of the back EMF under $m<0.5$ is coincident with the line of the modulated ZSV, thus the maximum k is acquired as 0.166 when m is less than 0.5. As the modulation index m grows beyond 0.5, the maximum tolerable k is decreased. For example, when m increases from 0.577 to 0.652, the maximum tolerable k is compressed from 0.1 to 0.05. From the above-mentioned analysis, it can be concluded that the higher the third flux linkage component in the motor, the smaller the region of ZSV that can be modulated. For a particular OW-PMSM with a given k under the tolerable range, a maximum m can always be expected so that ZSC can be effectively suppressed.

IV. Experimental Analysis

In this section, the experiments have been validated on a 1.25-kW OW-PMSM with a common dc bus. The experimental platform is presented in Fig. 13 , which is constructed on the basis of the DSP TMS320F28335 chip. Two control units shown in the upper left corner of Fig. 13 are utilized to drive the OW-PMSM and loading motor. The dc bus voltage is 220 V and the detailed parameters of the motor are shown in Table II. The control frequency is set as 15 kHz.

A. Steady-State Results

First, in order to test the feasibility of the proposed ZSC suppression strategy, an experimental comparison of ZSC suppression is conducted with the conventional DPCC without

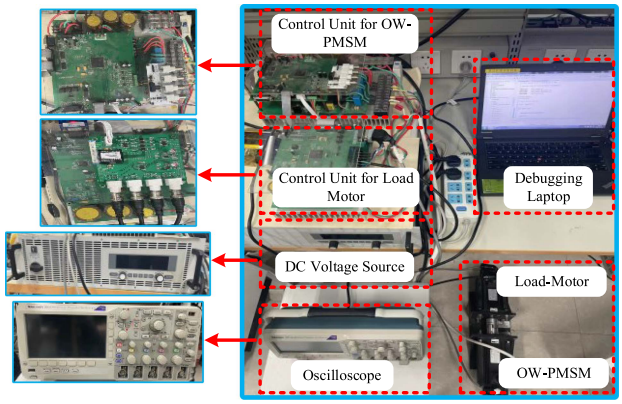

Fig. 13. Presentation of the experimental platform.

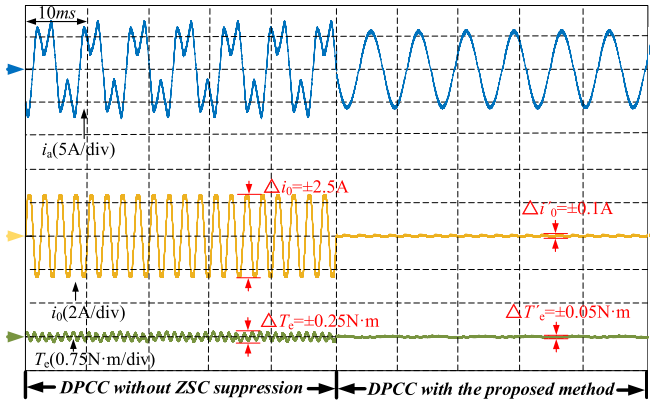

Fig. 14. Comparison of ZSC suppression between the conventional DPCC and the proposed method.

TABLE II
OW-PMSM Parameters

Parameters	Value	Parameters	Value
U_{dc}(V)	220	ψ_{f3} (Wb)	0.0059
R (Ω)	1.8	P_N(kW)	1.25
L_q (mH)	6.6	T_N (N•m)	5
L_d (mH)	6.6	n_N (r/min)	2000
L_0 (mH)	5.6	f(kHz)	15
ψ_f (Wb)	0.325		

redistributed reference voltage. In the conventional DPCC, the reference voltage is equally distributed to the dual-inverter. The experimental results with the speed of 500 r/min and rated load 5 N·m are shown in Fig. 14, from which it can be seen that the phase current of the conventional DPCC without ZSC suppression has undergone severe distortion and the ZSC ripple has reached ±2.5 A. The larger ZSC would increase the extra loss, which is not favorable for the long-term operation of the motor. Fortunately, after applying the proposed method with ZSC suppression, the ZSC ripple is reduced from ±2.5 to ±0.1 A. As a result, a standard sinusoidal phase current can be obtained. As the ZSC is suppressed, the electromagnetic torque ripple is reduced from ±0.25 to ±0.05 N·m, resulting in a smooth torque output.

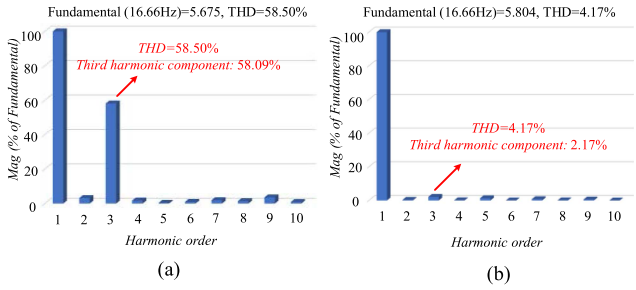

Fig. 15. Harmonic analysis. (a) Conventional DPCC without ZSC suppression. (b) Proposed method.

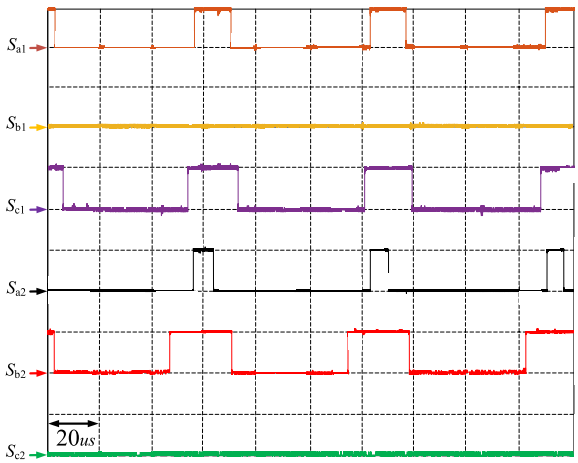

Fig. 16. Switching pulses of the upper bridge arm for dual-inverter.

Fig. 15 gives the phase current THD and harmonic analysis within two methods. As the main component of current harmonics, the third harmonic that constitutes the ZSC must be restrained and eliminated in the OW-PMSM with a common dc bus. It can be seen in Fig. 15 that, with the suppression of ZSC, the phase current THD is reduced from 58.50% to 4.17%, in which the third harmonic component is effectively suppressed from 58.09% to 2.17%.

Fig. 16 gives the switching pulses of the upper bridge arm for dual-inverter, from which it can be seen that, due to the abandonment of the zero VV $u_7(111)$, one-phase switching tubes are always clamped at 0 for a given control period. As a result, the switching frequency of the dual-inverter can be effectively reduced by 33% with respect to the conventional SVPWM, which is consistent with the theoretical analysis of Module B.

In addition, to demonstrate comprehensively the proposed method, the comparative experiments with the modulation strategy in [25] (named Method I), [26] (named Method II), [12] (named Method III), and the proposed method are implemented. The comparison of phase current THD at rated load 5 N·m and full-speed conditions (500, 1000, 1500, 2000 r/min) is demonstrated in Fig. 17, from which it can be seen that the phase current THD of the Method I is relatively high due to the application of the unilateral four-segment-mode. Comparatively, the phase current THD of the other three methods during the full-speed range is at a lower level. In addition, at low- and medium-speed

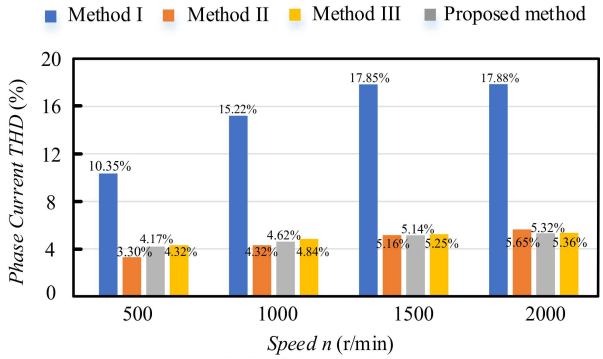

Fig. 17. Comparison of current THD within four methods.

intervals, the phase current THD of the Method II is the lowest among the four methods. The reason for this is that the VV acting at low speed is mainly zero VV, and the nonzero VV has a shorter duration of action. Thus, there is enough time for allocating the zero VV $u_0(000)$ and $u_7(111)$ to suppress the ZSC for good steady-state performance during one control period. However, at high-speed intervals, the duration of nonzero VV is extended, and the remaining space for allocating the zero VV is compressed or even under-allocated, so the phase current THD of the four methods are gradually close to each other.

Fig. 18 demonstrates the steady-state waveforms for the four methods at a rated speed 2000 r/min with a rated load 5 N·m. On the one hand, the SVPWM technique is employed by both methods III and the proposed method, which produces a higher switching frequency than methods I and II. The multiple switching of VV generates more dead zones for the inverter. However, ZSV generated by the dead-zone effect is not considered in this article, which leads to the relatively higher ZSV in methods III and the proposed method. Thus, a lower ripple of ZSC is obtained in methods I and II. Nevertheless, the ZSC of the system is well-suppressed within all four methods. For example, with the motor running at the rated speed of 2000 r/min and the rated load of 5 N·m, the ZSC ripple of the proposed method is only ± 0.2 A. On the other hand, the zero VV reallocation strategy is both used in methods I and II. The application of the zero VV $u_7(111)$ in the modulation process would cause a relatively high CMV, which further induces shaft current as well as jeopardizes motor operation. The CMV from the four methods are shown at the bottom of Fig. 18. It can be seen that the CMV maximum of methods I and II are around 140 and 115 V, while the CMV maximum of methods III and the proposed method are controlled to be about 70 V. The discard of zero VV $u_7(111)$ greatly reduces the CMV of the system, which is important for the long-term operation in high-power OW-PMSM.

Fig. 19 illustrates the waveforms of the weighting factor x at full-speed condition and rated load 5 N·m. It can be seen from Fig. 19 that the weighting factor x always fluctuates between 0.35 and 0.65 at both low- and high-speed conditions, which satisfies $0<x<1$. The over-modulation phenomenon does not occur. However, when the modulation index m is greater than the maximum allowable modulation index of 0.75, ZSV cannot be accurately generated. Fig. 20 illustrates the current waveform

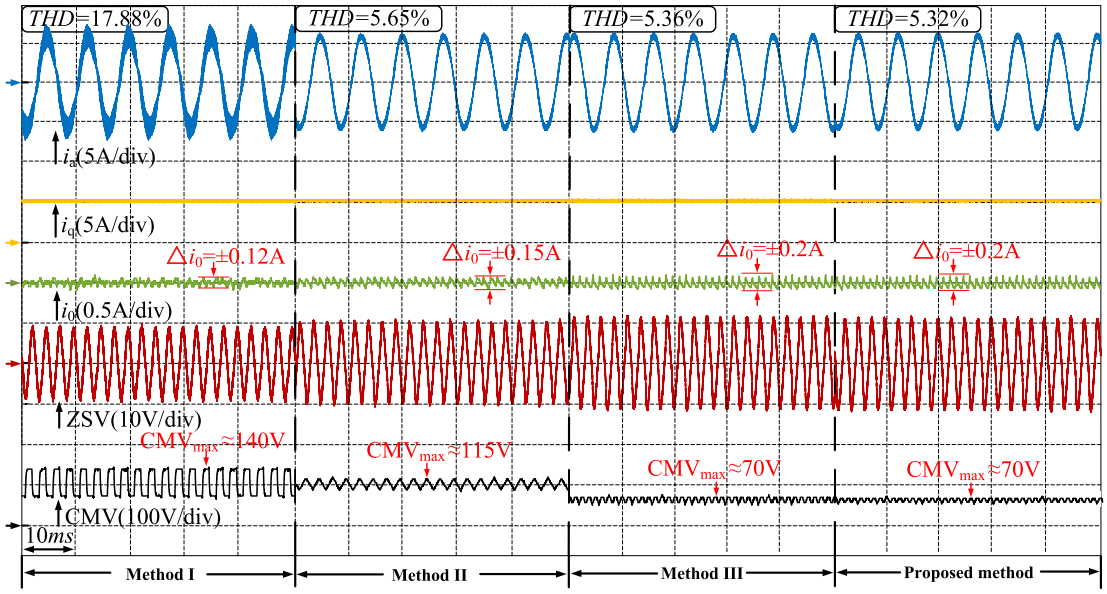

Fig. 18. Steady-state performance with a rated load of 5 N·m and the speed of 2000 r/min.

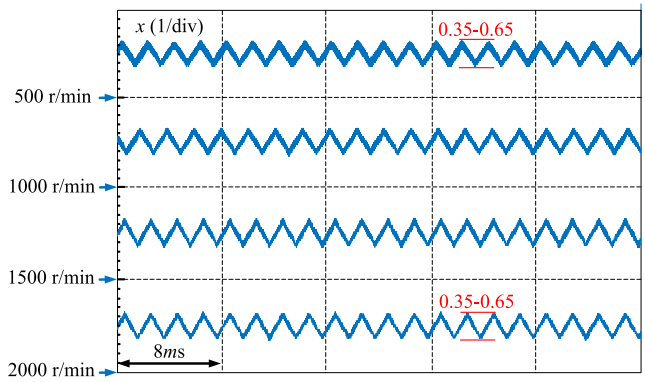

Fig. 19. Value of the weighting factor x under full-speed operating conditions at rated load 5 N·m.

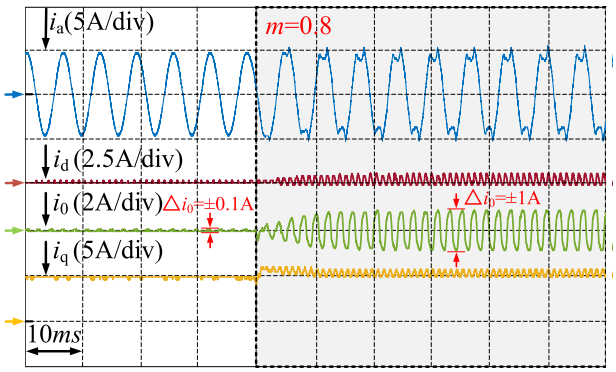

Fig. 20. Overmodulation when $m = 0.8$.

when m is 0.8, from which it can be seen that the phase current is distorted in this case and the ripple of the dq-axes current shows an increase in varying degrees. In addition, the ZSC ripple is increased from ±0.1 to ±1 A. ZSC cannot be effectively suppressed, which is limited by the ZSV modulation. Fortunately, the over-modulation can be compensated by using a larger dc bus voltage, which provides a wider modulation range.

B. Dynamic Results

The dynamic speed response waveforms of the four methods when the speed suddenly increases from 1000 to 1500 r/min with a rated load 5 N·m are demonstrated in Fig. 21, from which it can be seen that, under the sudden change of speed, all the four methods present good speed response-ability, and the real speed can track the reference value rapidly. However, due to the hysteresis of the PI regulator and the limitation of bandwidth, the speed up-time of Method III has reached 170 ms, which is slightly higher than the 160 ms of the other three methods.

Fig. 22 illustrates the dynamic variable load waveforms when the load suddenly changes from 3 to 5 N·m at the speed of 1000 r/min. It can be seen that, when the load is changed abruptly, the q-axis current i_q is able to quickly track its reference i_{qref} without static difference for four methods. Besides, similar to the dynamic performance as in the case of variable speed, the rise time of the current from dynamic to steady-state is about 130 ms within methods I, II, and the proposed method, whereas the rise time of the current in Method III is increased to 180 ms.

From the above-mentioned dynamic experiments with variable speed and load, it can be seen that a better dynamic performance is obtained in the proposed method.

C. Program Execution Time

Good dynamic and steady-state properties are essential performance metrics for a given control method, however, an extremely short program execution time is beneficial to enhance the implementation efficiency of the designed controller. The

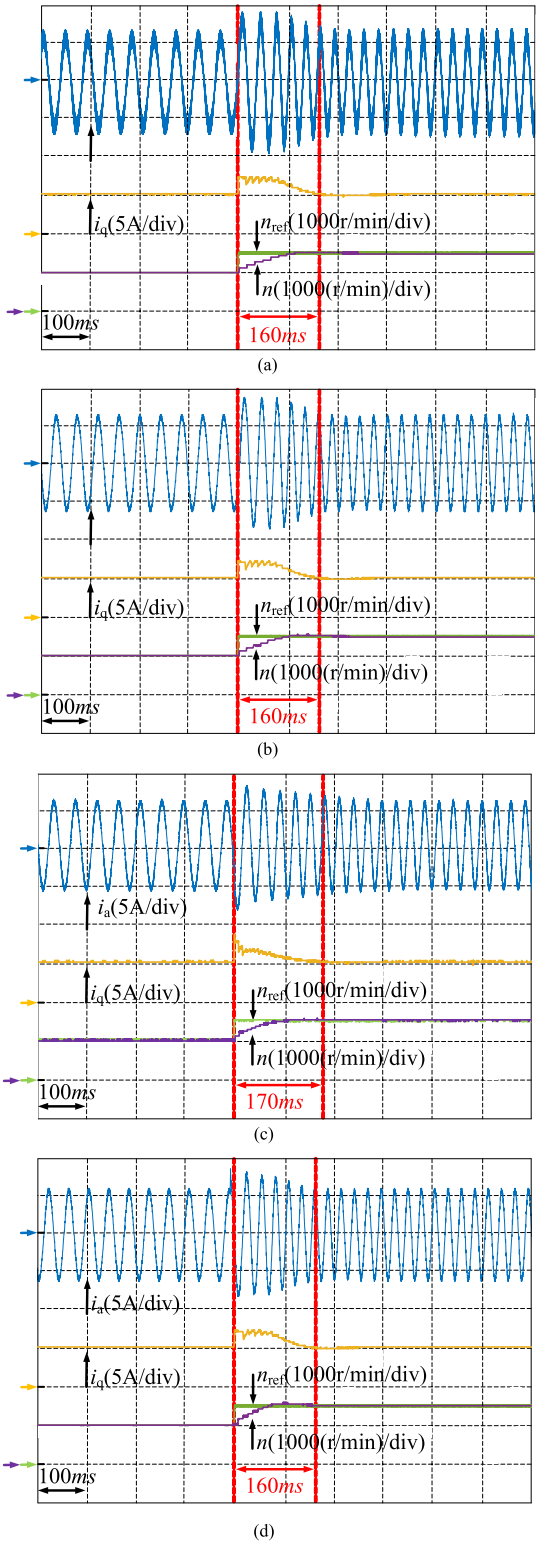

Fig. 21. Dynamic performance when the speed suddenly changes from 1000 to 1500 r/min with a rated load 5 N·m. (a) Method I. (b) Method II. (c) Method III. (d) Proposed method.

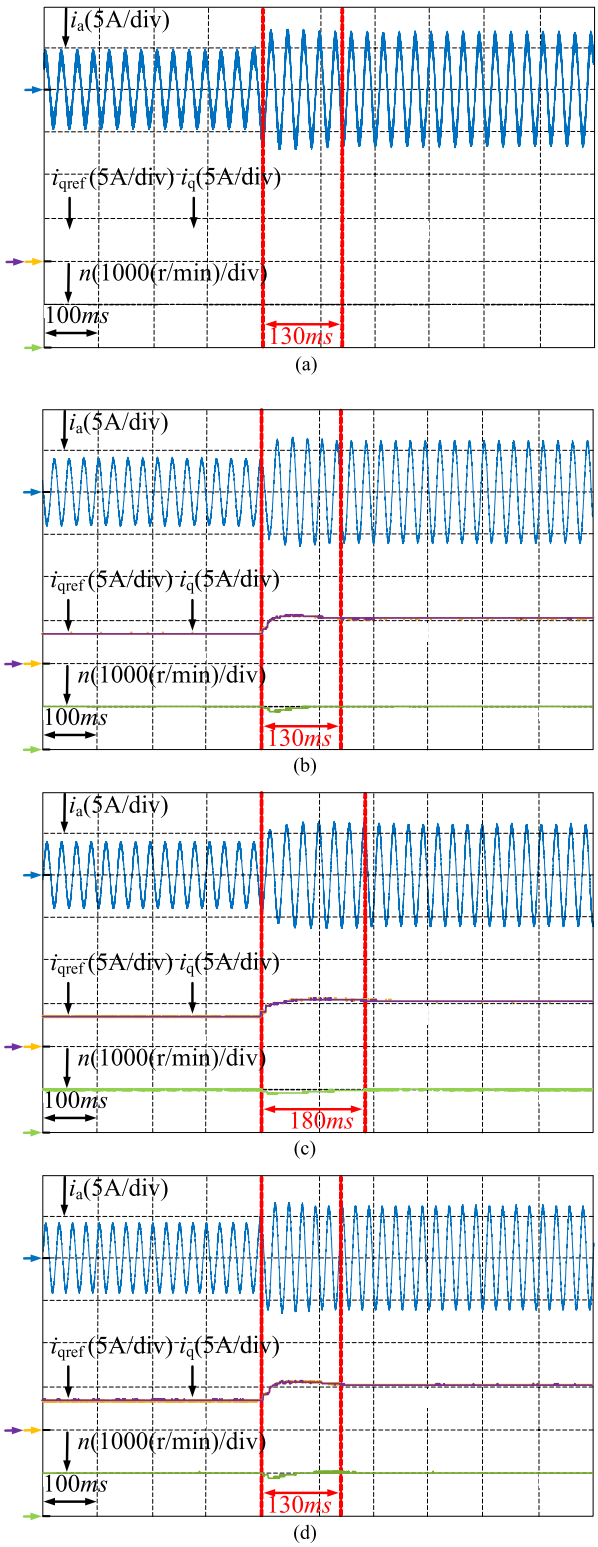

Fig. 22. Dynamic performance when the load suddenly changes from 3 to 5 N·m at the speed of 100 r/min. (a) Method I. (b) Method II. (c) Method III. (d) Proposed method.

TABLE III
COMPARISON OF PROGRAM EXECUTION TIMES FOR THE FOUR METHODS

Control method	Method I	Method II	Method III	Proposed method
Execution time	31.05 μs	35.82 μs	31.9 μs	29.17 μs

SWPWM module, as the most important part of the DPCC, is relatively time-consuming to implement. Therefore, simplifying the modulation strategy in DPCC as much as possible is prominent to reduce the amount of computation. The comparison of the computational burden of the four control methods is shown in Table III. It can be seen in Table III that the program execution time of Method II has reached 35.82 μs due to the complexity of the four-segment-mode-based modulation strategy, which is the most time-consuming among the four methods. However, only one weighting factor x needs to be resolved without significantly increasing the complexity of SVPWM, the computational burden of the proposed method can be further reduced compared to the other three methods.

V. CONCLUSION

In this article, a simple DPCC method is put forward for OW-PMSM drives with a common dc bus. The effectiveness and superiority have been experimentally verified in a 1.25-kW OW-PMSM. The main contributions of this work can be summarized as follows.

1) A reference voltage redistribution strategy is put forward, which keeps the ZSV and the third harmonic back EMF always in dynamic balance. As a result, ZSC can be completely suppressed. Besides, the CMV, which jeopardizes the long-term operation of the motor, can be further reduced by omitting the modulation of $u_7(111)$.
2) The switching frequency of the dual-inverter is effectively reduced by 33% compared to conventional SVPWM with six-time switching action.
3) Compared with the PI or PIR controller, the proposed DPCC can avoid the tedious and time-consuming parameter adjustment work, and a better dynamic performance can be obtained. In addition, the computational burden of the system is further reduced compared to the existing methods.

REFERENCES

[1] S. Li and Z. Liu, "Adaptive speed control for permanent-magnet synchronous motor system with variations of load inertia," *IEEE Trans. Ind. Electron.*, vol. 56, no. 8, pp. 3050–3059, Aug. 2009, doi: 10.1109/TIE.2009.2024655.

[2] H. Kim, J. Son, and J. Lee, "A high-speed sliding-mode observer for the sensorless speed control of a PMSM," *IEEE Trans. Ind. Electron.*, vol. 58, no. 9, pp. 4069–4077, Sep. 2011, doi: 10.1109/TIE.2010.2098357.

[3] X. Zhang, L. Sun, K. Zhao, and L. Sun, "Nonlinear speed control for PMSM system using sliding-mode control and disturbance compensation techniques," *IEEE Trans. Power Electron.*, vol. 28, no. 3, pp. 1358–1365, Mar. 2013, doi: 10.1109/TPEL.2012.2206610.

[4] S. Morimoto, K. Kawamoto, M. Sanada, and Y. Takeda, "Sensorless control strategy for salient-pole PMSM based on extended EMF in rotating reference frame," *IEEE Trans. Ind. Appl.*, vol. 38, no. 4, pp. 1054–1061, Jul./Aug. 2002, doi: 10.1109/TIA.2002.800777.

[5] J. Ewanchuk, J. Salmon, and C. Chapelsky, "A method for supply voltage boosting in an open-ended induction machine using a dual inverter system with a floating capacitor bridge," *IEEE Trans. Power Electron.*, vol. 28, no. 3, pp. 1348–1357, Mar. 2013, doi: 10.1109/TPEL.2012.2207741.

[6] H. Zhan, Z.-Q. Zhu, and M. Odavic, "Analysis and suppression of zero sequence circulating current in open winding PMSM drives with common DC bus," *IEEE Trans. Ind. Appl.*, vol. 53, no. 4, pp. 3609–3620, Jul./Aug. 2017, doi: 10.1109/TIA.2017.2679678.

[7] X. Zhang and K. Wang, "Current prediction based zero sequence current suppression strategy for the semicontrolled open-winding PMSM generation system with a common DC bus," *IEEE Trans. Ind. Electron.*, vol. 65, no. 8, pp. 6066–6076, Aug. 2018, doi: 10.1109/TIE.2017.2784353.

[8] S. Liu, C. Liu, Y. Huang, and H. Zhao, "Model predictive two-target current control for OW-PMSM," *IEEE Trans. Power Electron.*, vol. 36, no. 3, pp. 3224–3235, Mar. 2021, doi: 10.1109/TPEL.2020.3016714.

[9] N. Chai and W. Hu, "A fault-tolerant scheme against the open-switch failure in open-end winding PMSM system with isolated DC bus," *IEEE Trans. Energy Convers.*, vol. 38, no. 3, pp. 2227–2230, Sep. 2023, doi: 10.1109/TEC.2021.3115975.

[10] Y. Chen, X. Wang, X. Meng, M. He, D. Xiao, and Z. Wang, "A universal model predictive control strategy for dual inverters fed OW-PMSM drives," *IEEE Trans. Power Electron.*, vol. 38, no. 6, pp. 7575–7585, Jun. 2023, doi: 10.1109/TPEL.2023.3260305.

[11] C. Sun, D. Sun, Z. Zheng, and H. Nian, "Simplified model predictive control for dual inverter-fed open-winding permanent magnet synchronous motor," *IEEE Trans. Energy Convers.*, vol. 33, no. 4, pp. 1846–1854, Dec. 2018, doi: 10.1109/TEC.2018.2841012.

[12] W. Hu, H. Nian, and D. Sun, "Zero-sequence current suppression strategy with reduced switching frequency for open-end winding PMSM drives with common DC bus," *IEEE Trans. Ind. Electron.*, vol. 66, no. 10, pp. 7613–7623, Oct. 2019, doi: 10.1109/TIE.2018.2881945.

[13] Y. Kawabata, M. Nasu, T. Nomoto, E. C. Ejiogu, and T. Kawabata, "High-efficiency and low acoustic noise drive system using open-winding AC motor and two space-vector-modulated inverters," *IEEE Trans. Ind. Electron.*, vol. 49, no. 4, pp. 783–789, Aug. 2002, doi: 10.1109/TIE.2002.801059.

[14] V. T. Somasekhar et al., "PWM inverter switching strategy for a dual two-level inverter fed open-end winding induction motor drive with a switched neutral," *IEE Proc.-Electric Power Appl.*, vol. 149, no. 2, pp. 152–160, 2002.

[15] V. T. Somasekhar et al., "Dual two-level inverter scheme for an open-end winding induction motor drive with a single DC power supply and improved DC bus utilisation," *IEE Proc.-Electric Power Appl.*, vol. 151, no. 2, pp. 230–238, 2004.

[16] Y. Zhou and H. Nian, "Zero-sequence current suppression strategy of open-winding PMSG system with common DC bus based on zero vector redistribution," *IEEE Trans. Ind. Electron.*, vol. 62, no. 6, pp. 3399–3408, Jun. 2015, doi: 10.1109/TIE.2014.2366715.

[17] Q. An, J. Liu, Z. Peng, L. Sun, and L. Sun, "Dual-space vector control of open-end winding permanent magnet synchronous motor drive fed by dual inverter," *IEEE Trans. Power Electron.*, vol. 31, no. 12, pp. 8329–8342, Dec. 2016, doi: 10.1109/TPEL.2016.2520999.

[18] W. Hu, H. Nian, and T. Zheng, "Torque ripple suppression method with reduced switching frequency for open-winding PMSM drives with common DC bus," *IEEE Trans. Ind. Electron.*, vol. 66, no. 1, pp. 674–684, Jan. 2019, doi: 10.1109/TIE.2018.2833803.

[19] W. Hu, C. Ruan, H. Nian, and D. Sun, "Zero-sequence current suppression strategy with common-mode voltage control for open-end winding PMSM drives with common DC bus," *IEEE Trans. Ind. Electron.*, vol. 68, no. 6, pp. 4691–4702, Jun. 2021, doi: 10.1109/TIE.2020.2988221.

[20] C. Liu and J. Shang, "Three-dimension space vector based finite control set method for OW-PMSM with zero-sequence current suppression and switching frequency reduction," *IEEE Trans. Power Electron.*, vol. 36, no. 12, pp. 14074–14086, Dec. 2021, doi: 10.1109/TPEL.2021.3087015.

[21] X. Zhang and C. Zhang, "Model predictive control for open winding PMSM considering dead-zone effect," *IEEE J. Emerg. Sel. Topics Power Electron.*, vol. 11, no. 1, pp. 874–885, Feb. 2023, doi: 10.1109/JESTPE.2022.3207186.

[22] L. Cheng, H. Jianhui, and S. Jing, "Dual-vector predictive current control of open-end winding PMSM with zero-sequence current hysteresis control," *IEEE J. Emerg. Sel. Topics Power Electron.*, vol. 10, no. 1, pp. 184–195, Feb. 2022, doi: 10.1109/JESTPE.2021.3079638.

[23] S. Chen, W. Ding, X. Wu, R. Hu, and S. Shi, "Finite position set-phase-locked loop with low computational burden for sensorless control of PMSM drives," *IEEE Trans. Ind. Electron.*, vol. 70, no. 9, pp. 9672–9676, Sep. 2023, doi: 10.1109/TIE.2022.3215457.

[24] M. S. R. Saeed, W. Song, B. Yu, Z. Xie, and X. Feng, "Low-complexity deadbeat model predictive current control for open-winding PMSM drive with zero-sequence current suppression," *IEEE Trans. Transp. Electrific.*, vol. 7, no. 4, pp. 2671–2682, Dec. 2021, doi: 10.1109/TTE.2021.3071471.

[25] X. Zhang, H. Zhang, and K. Yan, "Hybrid vector model predictive control for open-winding PMSM drives," *IEEE Trans. Transp. Electrific.*, to be published, doi: 10.1109/TTE.2023.3308570.

[26] X. Zhang and H. Zhang, "Bilateral four-segment-mode model predictive control for open-winding PMSM drives," *IEEE Trans. Power Electron.*, vol. 38, no. 11, pp. 14410–14422, Nov. 2023, doi: 10.1109/TPEL.2023.3305294.

[27] S. Wang, S. Zhang, C. Zhang, X. Li, and Y. Dong, "An improved modulation scheme with better performance for open-winding permanent magnet synchronous motors drives," *IEEE Trans. Energy Convers.*, vol. 38, no. 2, pp. 1376–1386, Jun. 2023, doi: 10.1109/TEC.2022.3228544.

[28] X. Yuan, C. Zhang, and S. Zhang, "A novel deadbeat predictive current control scheme for OEW-PMSM drives," *IEEE Trans. Power Electron.*, vol. 34, no. 12, pp. 11990–12000, Dec. 2019, doi: 10.1109/TPEL.2019.2904387.

[29] X. Lin, W. Huang, and L. Wang, "SVPWM strategy based on the hysteresis controller of zero-sequence current for three-phase open-end winding PMSM," *IEEE Trans. Power Electron.*, vol. 34, no. 4, pp. 3474–3486, Apr. 2019, doi: 10.1109/TPEL.2018.2856372.

[30] J. Kalaiselvi and S. Srinivas, "Bearing currents and shaft voltage reduction in dual-inverter-fed open-end winding induction motor with reduced CMV PWM methods," *IEEE Trans. Ind. Electron.*, vol. 62, no. 1, pp. 144–152, Jan. 2015, doi: 10.1109/TIE.2014.2336614.

[31] A. K. Datta, M. Dubey, and S. Jain, "Effect of static power supply in alternator used for short-circuit testing-observation of shaft voltage," *IEEE Trans. Power Electron.*, vol. 29, no. 11, pp. 6074–6080, Nov. 2014, doi: 10.1109/TPEL.2014.2300185.

Han Zhang was born in Anhui, China, in 1998. He received the B.S. degree in electrical engineering from the Chizhou University, Chizhou, China, in 2021. He is currently working toward the M.S. degree in electrical engineering at North China University of Technology, Beijing, China.

His current research interest focuses on ac motor drives.

Xiaoguang Zhang (Senior Member, IEEE) received the B.S. degree in electrical engineering from the Heilongjiang Institute of Technology, Harbin, China, in 2007, and the M.S. and Ph.D. degrees in electrical engineering from the Harbin Institute of Technology, in 2009 and 2014, respectively.

He is currently a full Professor with the North China University of Technology, and the Director of Beijing Power Electronics and Electrical Transmission Engineering Research Center. From 2012 to 2013, he was a Research Associate with Wisconsin Electric Machines and Power Electronics Consortium (WEMPEC), University of Wisconsin–Madison, Madison, WI, USA. He has authored or coauthored more than 100 technical papers in the area of motor drives.

Dr. Zhang is serving as an Associate Editor of IEEE TRANSACTIONS ON ENERGY CONVERSION and IET POWER ELECTRONICS. His current research interests include power electronics and electric machines drives.